Can. J. Remote Sensing, Vol. 30, No. 5, pp. 731–742, 2004

Spatial distribution of net primary productivity and evapotranspiration in Changbaishan Natural Reserve, China, using Landsat ETM+ data

Rui Sun, J.M. Chen, Qijiang Zhu, Yuyu Zhou, J. Liu, Jiangtao Li, Suhong Liu, Guangjian Yan, and Shihao Tang

Abstract. Remote sensing has been a useful tool to monitor net primary productivity (NPP) and evapotranspiration (ET). In this paper, based on field measurements and Landsat enhanced thematic mapper plus (ETM+) data, NPP and ET are estimated in 2001 in the Changbaishan Natural Reserve, China. Maps of land cover, leaf area index, and biomass of this forested region are first derived from ETM+ data. With these maps and additional soil texture and daily meteorological data, NPP and ET maps are produced for 2001 using the boreal ecosystem productivity simulator (BEPS). The results show that the estimated and observed NPP values for forest agree fairly well, with a mean relative error of 8.6%. The NPP of mixed forests is the highest, with a mean of 500 g C $m^{-2}{\cdot}a^{-1}$, and that of alpine tundra and shrub is the lowest, with a mean of 136 g C $m^{-2}{\cdot}a^{-1}$. Unlike the spatial pattern of NPP, the annual ET changes distinctly with altitude from greater than 600 mm at the foot of the mountain to about 200 mm at the top of the mountain. ET is highest for broadleaf forests and lowest for urban and built-up areas.

Résumé. La télédétection est un outil utile pour faire le suivi de la productivité primaire nette (PPN) et de l'évapotranspiration (ET). Dans cet article, basé sur des mesures de terrain et des données ETM+ de Landsat, on fait l'estimation de la PPN et de l'ET pour l'année 2001, dans la réserve naturelle de Changbaishan, en Chine. Des cartes du couvert, d'indice de surface foliaire et de biomasse de cette région forestière sont dérivées au départ des données ETM+. À l'aide de ces cartes, de données supplémentaires sur la texture du sol et des données météorologiques journalières, on a produit des cartes de PPN et ET à l'aide du simulateur BEPS (« boreal ecosystem productivity simulator ») pour 2001. Les résultats montrent que les valeurs estimées et observées de PPN de la forêt concordent plutôt bien, avec une erreur relative moyenne de 8,6%. La valeur de PPN des forêts mixtes est plus élevée, avec une moyenne de 500 g C $m^{-2}{\cdot}a^{-1}$, alors que la valeur de PPN de la toundra alpine et des arbustes est plus faible, avec une moyenne de 136 g C $m^{-2}{\cdot}a^{-1}$. Contrairement au patron spatial de PPN, la valeur annuelle de ET change de façon marquée avec l'altitude à partir de 600 nm, au pied de la montagne, à environ 200 nm au sommet de la montagne. La valeur de ET est plus élevée pour les forêts de feuillus et à son plus bas pour les zones urbaines et construites.
[Traduit par la Rédaction]

Introduction

As a major part of terrestrial ecosystems, vegetation plays an important role in the energy, matter, and momentum exchange between the land surface and the atmosphere. Through the process of photosynthesis, plants assimilate carbon in the atmosphere and incorporate it into the biomass, and part of the carbon is emitted into the atmosphere again through plant respiration (autotrophic respiration). The difference between photosynthesis and autotrophic respiration is the net primary productivity (NPP). As Changbaishan Natural Reserve is one of the most productive and undisturbed areas in China, it is of great interest in the studies of the terrestrial carbon cycle of the region and is also of significance in global carbon cycle research. A field experiment was conducted in 2002 to obtain the spatial pattern of NPP in Changbaishan Natural Reserve.

Many models have been established to estimate regional and global NPP and can be classified into three types: climate models, process models, and energy use efficiency models. Climate models estimate NPP by establishing the statistical relation between NPP and climate data (Rosenzweig, 1968; Lieth and Whittaker, 1975; Uchijima and Seino, 1985; Box, 1988). For example, the Miami model used the empirical relationship among NPP, annual mean temperature, and precipitation to estimate global terrestrial NPP (Lieth and Whittaker, 1975).

Process models estimate NPP based on plant physiological and ecological processes (Fung et al., 1987; Running and Coughlan, 1988; King et al., 1989; Melillo et al., 1993; Foley,

Received 15 November 2003. Accepted 1 April 2004.

R. Sun,[1] Q. Zhu, Y. Zhou, J. Li, S. Liu, G. Yan, and S. Tang. Research Center for Remote Sensing and GIS, School of Geography, Beijing Normal University, Beijing, 100875, China, State Key Laboratory of Remote Sensing Science, Beijing, 100875, China, and Beijing Key Laboratory for Remote Sensing of Environment and Digital Cities, Beijing, 100875, China.

J.M. Chen. Department of Geography and Program in Planning, University of Toronto, Toronto, ON M5S 3G3, Canada.

J. Liu. Department of Physics, University of Toronto, Toronto, ON M5S 1A7, Canada.

[1]Corresponding author (e-mail: sunrui@bnu.edu.cn).

1994; Bonan, 1995; Liu et al., 1997). Photosynthesis, evapotranspiration, autotrophic respiration, and dry matter partition have to be considered, and there are usually many parameters in these models. These models can be run at small time steps. In combination with general circulation models (GCMs), process models can be effectively used to evaluate the effect of climate change on regional and global NPP.

The availability of multitemporal and multispectral remote sensing information has enabled measurement and monitoring of land surface parameters such as leaf area index (LAI), phenology, and fraction of absorbed photosynthetic active radiation (FPAR) by vegetation, which help us to study the spatial distribution and seasonal and interannual changes in NPP. The advanced very high resolution radiometer (AVHRR) on the National Oceanic and Atmospheric Administration (NOAA) satellite and moderate resolution imaging spectrometer (MODIS) on the Terra and Aqua satellites provide daily, global, red and near-infrared reflectance data, from which cloud-free, near-nadir composite data can be formed at a frequency of once every month or every 10 days. These data have been widely used to estimate plant production. Because there exist strong relationships between FPAR and vegetation indices (Asrar et al., 1984; Gallo et al., 1985; Bartlett et al., 1990), especially the simple ratio (SR = NIR/VIS, where NIR and VIS are the reflectance in the near-infrared and visible bands, respectively) and the normalized difference vegetation index (NDVI = (NIR – VIS)/(NIR + VIS)), SR and NDVI have been used to determine FPAR (Potter et al., 1993; Law and Waring, 1994; Ruimy and Saugier, 1994; Field et al., 1995; Prince and Goward, 1995; Sun and Zhu, 2001).

Energy use efficiency models use energy use efficiency and the relationship between vegetation index and FPAR to estimate radiation absorbed by plants and therefore NPP. Because an energy use efficiency model is simple and uses remotely sensed data, it is widely used. Meanwhile, remote sensing data have also been used in process models to provide input data, such as LAI and vegetation type (Sellers et al., 1996; Liu et al., 1997; 2002).

In China, there has been much research on NPP models and their applications. For example, Luo et al. (1998) and Li et al. (1998) established relationships between NPP and air temperature, rainfall, and evapotranspiration to estimate NPP. Zhu (1993) and Zhou and Zhang (1996) improved the Chikugo model (Uchijima and Seino, 1985) and analyzed the effect of climate change on NPP in China. In recent years, process models in conjunction with remote sensing data have also been used to analyze the spatial pattern of NPP in China (Piao et al., 2001; Sun and Zhu, 2001; Yu et al., 2001; Chen et al., 2002a; Lu and Ji, 2002; Zhang et al., 2003). Because there are few ground NPP data used to validate model results, however, especially at the scale of remote sensing pixels, the magnitude of NPP for China's ecosystems and for any given region in China varied greatly among the published results. To obtain reliable values of NPP for a given region, it is necessary to carry out field experiments to obtain NPP data for ground plots and then scale them up to coarse-resolution remote sensing pixels (~1000 m) using high-resolution (~30 m) imagery. The objective of this paper is to produce high-resolution NPP and evapotranspiration (ET) maps using the boreal ecosystem productivity simulator (BEPS) model and Landsat enhanced thematic mapper plus (ETM+) data based on field measurements. These maps can then be used to validate and improve other model results at coarser resolutions.

Field experiment

Experimental site

The experimental site is located in the north slope of Changbaishan Natural Reserve and nearby areas in the southeast of Jilin Province, China (41°42′N–42°10′N, 127°38′E–128°10′E) (**Figure 1**). The site has an elevation varying from 720 to 2691 m above sea level and a temperate continental mountainous climate. Annual rainfall is about 700 mm at lower elevations and increases to about 1400 mm at Tianchi Lake, the top of Changbaishan Mountain. The mean annual air temperature decreases from +4.9 °C at the foot of the mountain to –7.3 °C at the top.

Influenced by the climate, the Changbaishan Natural Reserve has obvious vertical vegetation zones, including Korean pine and broadleaf mixed forest at elevations from 720 to 1100 m, spruce and fir forest at elevations from 1100 to 1800 m, *Betula ermanii* forest in the subalpine zone at elevations from 1800 to 2100 m, and alpine tundra at elevations above 2100 m. The Korean pine and broadleaf mixed forest is the dominant vegetation type. The vegetation density varies with height, providing a large natural range for developing remote sensing algorithms of biophysical parameters. It is therefore also ideal for validating NPP and ET models.

LAI measurements

LAI was measured using a tracing radiation and architecture of canopies (TRAC) instrument, which can acquire the clumping index, an important factor in the calculation of LAI of coniferous forest. Taking into account the vegetation representation, vertical zones, and road access conditions, we chose 34 stands to carry out the LAI measurements. These stands are distributed evenly in each vertical zone (**Figure 2**). The main vegetation types include Korean pine and broadleaf mixed forest, poplar and birch forest, *B. ermanii* forest, spruce–fir forest, Korean pine forest, and transitional forest.

The LAI sampling area is 30 m × 30 m, which is equal to the grid size of the Landsat ETM+ data. In each stand, the canopy gap fraction and gap size distribution of four 30 m long lines were measured using TRAC. Auxiliary data such as longitude and latitude were obtained by global positioning system (GPS). After taking into account the element clumping index derived from the gap size distribution, LAI was calculated according to the measured canopy gap fraction.

Biomass and NPP measurements

The relative growth method was used to measure the biomass (Feng et al., 1999). The biomass of each part of a tree (stem, branch, leaf, root) was estimated from the tree height and the diameter at breast height (DBH) using a formula derived from the field measurements.

In our measurements, we selected 10 stands for measuring biomass (**Figure 2**), with a sampling area of 30 m × 30 m for each stand. The stands include *Pinus sylvestriformis* forest (one stand), Korean pine and broadleaf mixed forest (two stands), poplar and birch forest (two stands), spruce and fir forest (three stands), and *B. ermanii* forest (one stand). Structural parameters including DBH, height of each tree, and number of trees in each sampling area were measured. The biomass of each tree was then acquired based on species-specific relative growth formulas (Chen and Zhu, 1989). Lastly, the biomass for each sampling area was calculated from the measured structural parameters.

NPP includes three components: change in live biomass, mortality, and biomass eaten by animals. The last component occupies a small proportion in the total NPP, so it was ignored in our research. Tree mortality varies with stand age and can account for a significant fraction of annual biomass increment. As remote sensing based estimation does not include the reduction of NPP due to mortality, we have not included this component in our current study. The exclusion of this component enables us to use ground data for validating remote sensing based estimates. It is therefore necessary to consider this component in full carbon cycle modeling (Chen et al., 2003). Biomass increment data derived from the increment of DBH were used to calculate the NPP. The data of the increment of DBH were obtained from the tree ring samples (about 10 trees per stand were sampled, and two tree cores were taken for each tree). These DBH increment data were then used to estimate the increment of each biomass component of each tree from 2000 to 2001 acquired according to the relative growth formula. The NPP of a stand, i.e., the change of biomass between 2 years, was then estimated according to the number of trees in each sampling area. Lastly, the NPP of each stand in 2001 was calculated using this method.

Model description

The BEPS model was used in this study to estimate NPP and ET. BEPS was developed by Liu et al. (1997) based on the forest biogeochemical cycles (Forest-BGC) model of Running and Coughlan (1988). It implemented an advanced photosynthesis model with a new temporal and spatial scaling scheme (Chen et al., 1999). LAI and land cover needed in the model can be obtained from remote sensing data. This improvement successfully addressed the scaling problem from individual leaves to canopy by separating the canopy into sunlit and shaded leaf groups. An analytical solution was also developed to determine a simplified daily integral of the model of Farquhar et al. (1980) by considering the general diurnal patterns of meteorological variables. Therefore, the new daily canopy photosynthesis model not only captures the main effects of diurnal variations on photosynthesis, but also is computationally efficient for large-area applications.

The NPP is modeled in five steps. Step 1 is to estimate soil water balance based on the "bucket" model, which includes the calculations of snowmelt, canopy interception, ET, and overflow. A vegetated area is divided into three layers: overstory, understory, and soil. Evaporation and transpiration are calculated using the Penman–Monteith equation for each layer. Step 2 calculates the mesophyll conductance and the canopy stomatal conductance according to radiation, air temperature, vapor pressure deficit, leaf nitrogen concentration,

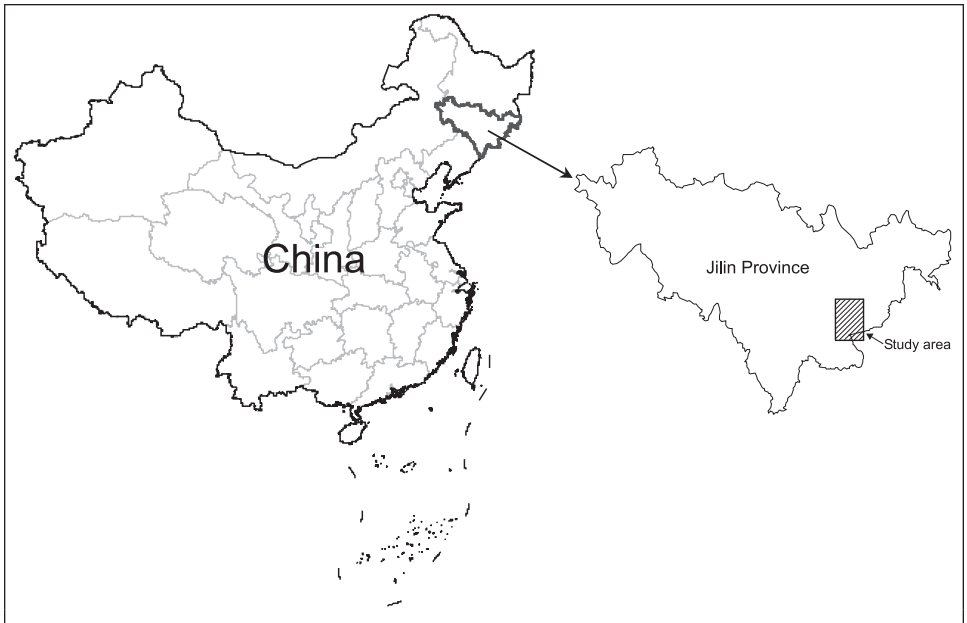

Figure 1. Location of the field experiment site.

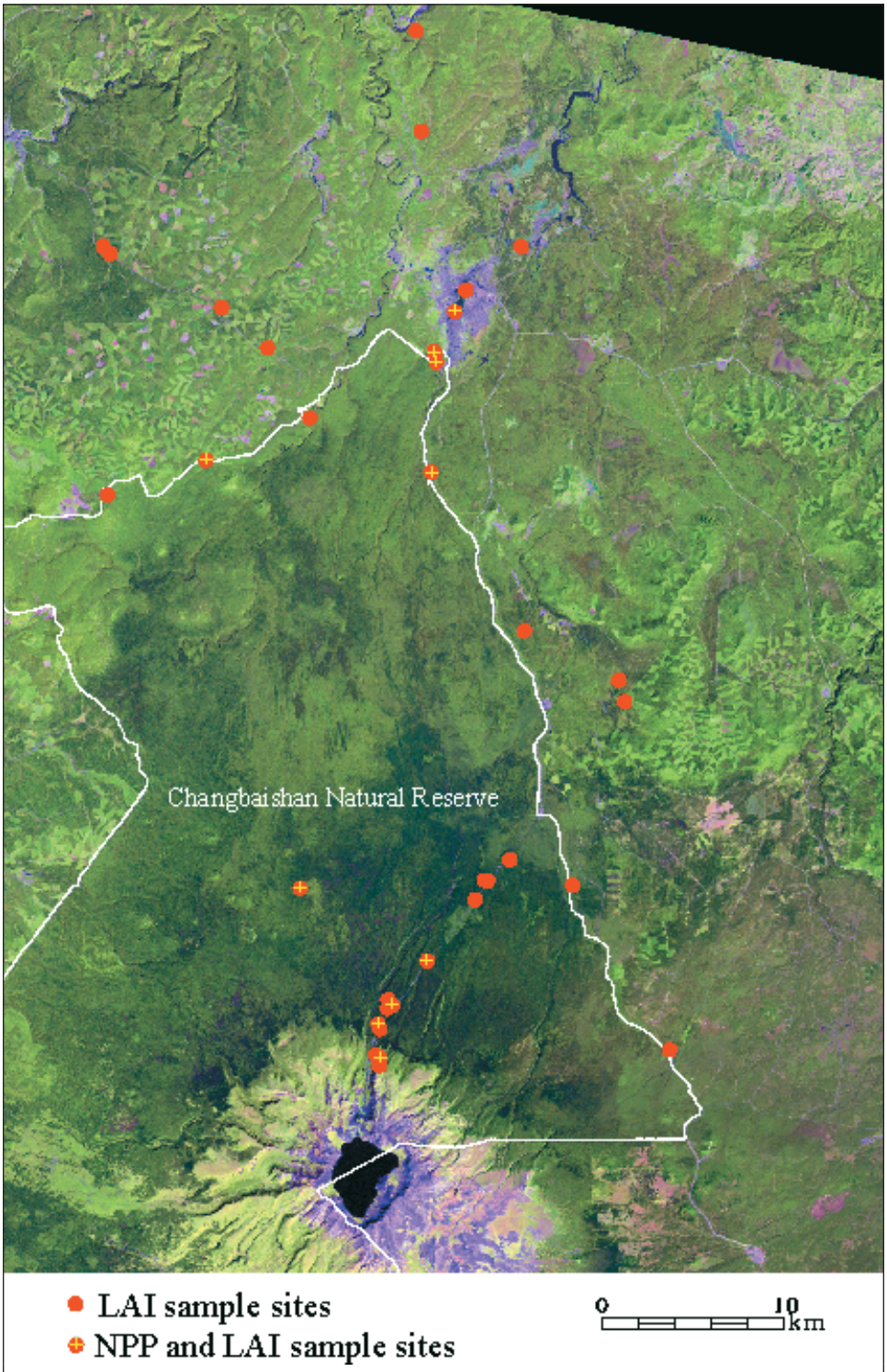

Figure 2. Locations of LAI and biomass measurement sites. The background is a color composite image of Landsat ETM+ data from 4 September 1999.

and leaf water potential. Daily gross photosynthesis or gross primary productivity (GPP) is calculated in step 3 as follows:

$$GPP = [\Delta CO_2 \times CC \times CM/(CC + CM)] \times LAI \times DAYL \quad (1)$$

where CC is the canopy stomatal conductance, CM is the mesophyll conductance, ΔCO_2 is the CO_2 gradient between leaf and air (calculated based on the model of Farquhar et al., 1980), LAI is the leaf area index, and DAYL is the day length. Equation (1) is implemented for sunlit and shaded leaf groups separately. Daily maintenance respiration is calculated and

subtracted from daily gross respiration in step 4. Based on respiration coefficients, biomass, and temperature, daily maintenance respiration of stems, leafs, and roots is calculated separately in step 4. The final step is to sum the daily results in step 4 for the whole year and subtract 20% (Raich et al., 1991; Ryan, 1991) of the yearly total for the growth respiration, leading to annual NPP.

The outputs of the BEPS model include annual and daily NPP, respiration, gross primary productivity (GPP), transpiration, and evaporation.

Input requirements for the model

The inputs to the BEPS model include land cover type, available soil water capacity, biomass, LAI, daily maximum and minimum air temperature, vapor pressure deficit, precipitation, and incident solar radiation. The meteorological data were obtained from meteorological stations, and LAI and land cover type maps were derived from remote sensing data.

Meteorological data and available soil water capacity

Meteorological data, including daily maximum and minimum air temperature, vapor pressure, and precipitation in 2001, were obtained from 28 meteorological stations in Jilin Province. The vapor pressure and precipitation data were interpolated to 30 m grids using the Kriging method. Air temperature varies largely with topography. Thus, when air temperature is interpolated to the grid data, the effects of topography must be taken into account so that the error associated with the interpolation can be minimized. The air temperatures from weather stations were first converted to "sea level air temperature" according to the altitude of the weather stations and then interpolated to 30 m grids using the Kriging method. With digital elevation model (DEM) data digitized from 1 : 50 000 scale topographic map, the gridded sea level air temperature images are further converted to the actual air temperature. The results of Weng and Sun (1984) showed that the lapse rate of air temperature in the Changbaishan Mountain area ranged from 0.4 °C/100 m in January to about 0.6 °C/100 m in July. We simply assumed that the lapse rate of air temperature is 0.5 °C/100 m throughout the year. The daily incident solar radiations were calculated from the DEM data, daily gridded precipitation, and maximum and minimum air temperature using the relationship established by Winslow et al. (2001).

The 1 : 250 000 scale soil texture map was used to produce the soil available water capacity (AWC) map. In this paper, we adopted the empirical relationship established by Saxton et al. (1986) between soil water content and soil grain size distribution to estimate AWC.

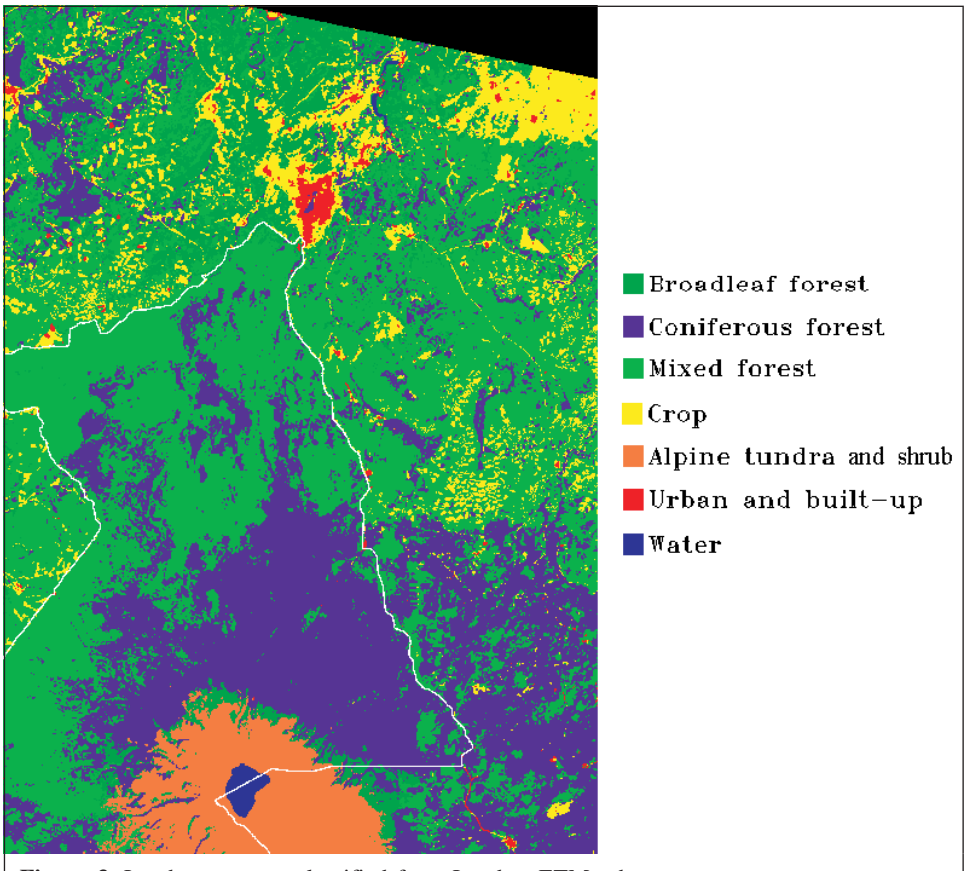

Figure 3. Land cover map classified from Landsat ETM+ data.

Remote sensing data processing

Landsat ETM+ data were acquired on 25 August 2002 during the time the field experiment was conducted. Because part of the image is contaminated by clouds, Landsat ETM+ data on 4 September 1999 were also selected to replace the data influenced by clouds. The two images were first georeferenced by the selected ground-control points from 1 : 50 000 scale maps. The accuracy of georeferencing is 0.8 pixels. Atmospheric correction was then performed using 6S software (Vermote et al., 1997) with near-realtime inputs of the precipitable water content, aerosol optical thickness from National Aeronautics and Space Administration (NASA) MODIS data product, and ozone data from total ozone mapping spectrometer (TOMS) data. After the atmospheric correction, the reflectance for each band is calculated and then used to produce the map of land cover, LAI, and aboveground biomass.

Land cover map

Integrating DEM data and using the maximum likelihood classification method, we classified the land cover of Changbaishan Natural Reserve and its surrounding area into seven types (**Figure 3**). The main land cover includes broadleaf forest, coniferous forest, mixed forest, crop, alpine tundra and shrub, urban and built-up, and water. As shown in **Figure 3**, mixed forest is the major vegetation type, occupying about 46% of the study area. Coniferous forest is the next most common vegetation type, occupying 29% of the study area. The broadleaf forest distributed at high altitude is *B. ermanii* forest, which is the transition vegetation between spruce–fir forest and alpine tundra.

LAI data

According to the reflectance data of bands 3, 4, and 5, two kinds of vegetation indices were computed, namely the simple ratio SR (SR = R_4/R_3, where R_3 and R_4 are the reflectances of bands 3 and 4, respectively) and the reduced simple ratio RSR (Brown et al., 2000), defined as follows:

$$\mathrm{RSR} = \mathrm{SR}[1 - (R_5 - R_{5\min})/(R_{5\max} - R_{5\min})] \quad (2)$$

where R_5 is the reflectance of band 5; and $R_{5\min}$ and $R_{5\max}$ are the minimum and maximum reflectances of band 5 and are defined as the 1% minimum and maximum cutoff points in the histograms of band 5 reflectance. The major advantages of RSR over SR are (Chen et al., 2002b) as follows: (*i*) the difference between cover types is very much reduced, so the accuracy of LAI retrieval for mixed cover types can be improved; and (*ii*) the background influence is suppressed using RSR because the SWIR band (band 5) is most sensitive to the amount of vegetation containing liquid water in the overstory.

The 3 pixel × 3 pixel averaged SR and RSR values for those pixels where LAI was measured were extracted and correlated with observed data (**Figure 4**). **Figure 4** shows that the relationship between LAI and RSR is better than that between LAI and SR. The relationship between LAI and SR is more sensitive to the background than that based on RSR, and the data are more scattered. Data points 1 and 2 in **Figure 4b** are obviously outliers and belong to *P. sylvestriformis* forest located in the centre of a town. The LAI value of this forest is above 5. The soil is very wet here, however, which decreases the band 4 reflectance, and the SR value is very low. By integrating reflectance data from band 5, the relationship is markedly improved. Thus the following relationship was used to estimate LAI of forest:

$$\mathrm{RSR} = 14.57 - 14.57 \exp(-0.13\mathrm{LAI}) \quad (3)$$

The LAI values of crop and tundra were estimated using the following equation (Chen et al., 2002b):

$$\mathrm{SR} = 14.5 - 13.5 \exp(-\mathrm{LAI}/1.6) \quad (4)$$

By using Equations (3) and (4), the LAI map on 25 August 2002 was produced (**Figure 5**). **Figure 5** shows that the LAI of forests increases with an increase in altitude, and the highest LAI value appears in the coniferous forest vegetation type.

To estimate NPP in 2001 using BEPS, we assume that the vegetation type and LAI on 25 August do not change between 2001 and 2002, so the LAI image was used directly to calculate NPP in 2001. Nevertheless, the annual NPP cannot be modeled

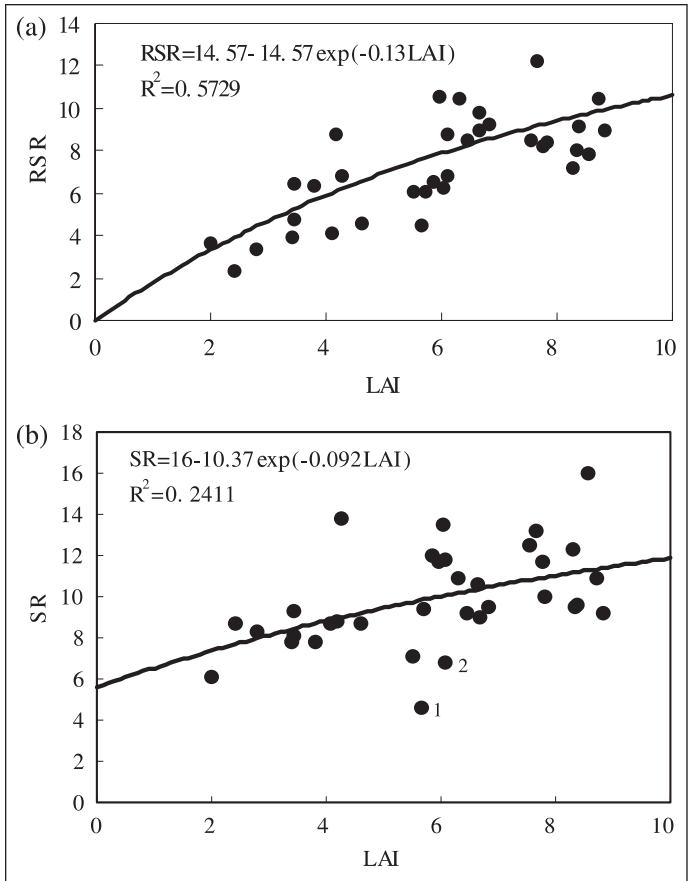

Figure 4. Relationship between LAI and vegetation indices RSR and SR.

using a single LAI image. To resolve this problem, we determined the period of vegetation growth and the period when LAI maintained the highest value for each pixel after analyzing the MODIS LAI data product in 2001. Lastly, we obtained the multitemporal LAI for the whole year using the temporal trends of MODIS LAI for each vegetation cover type.

Aboveground biomass

Aboveground biomass of forest is also needed for calculating maintenance respiration. Liu et al. (2002) analyzed the biomass and LAI data for Canada. The results demonstrated that the biomass could be estimated from LAI for different forest types. To acquire the spatial distribution of biomass in the study area, we compared the observed biomass data and 3 pixel × 3 pixel averaged LAI data from **Figure 5** (**Figure 6**). As shown in Figure 6, although there are two points considerably below the simulated curve (the two points are young disturbed stands: one point is *P. sylvestriformis* forest, which has been planted by man; and the other point is poplar and birch forest, which is secondary deciduous broadleaf forest), the determinant coefficient is high (R^2 = 0.7498). Thus, the aboveground biomass was estimated from LAI using the following equation:

$$W_g = -0.9944\mathrm{LAI}^2 + 42.481\mathrm{LAI} \quad (5)$$

where W_g is the aboveground biomass (t DW hm^{-2}). The units for W_g are further converted to t C hm^{-2} by multiplying by a factor of 0.5.

Results and discussion

Annual NPP and ET in 2001 were estimated using BEPS and the data described previously.

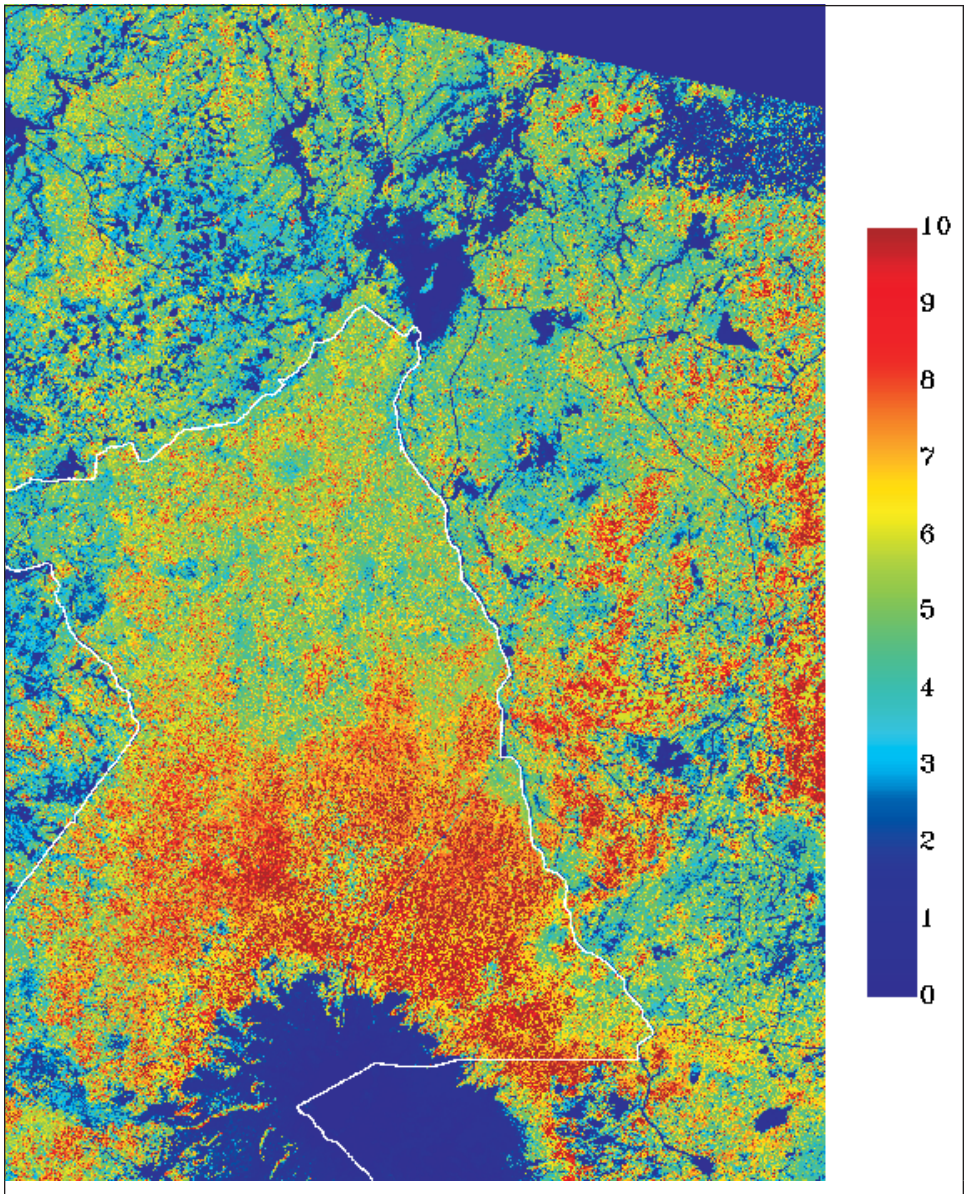

Figure 5. Spatial pattern of LAI in Changbaishan Natural Reserve on 25 August 2002.

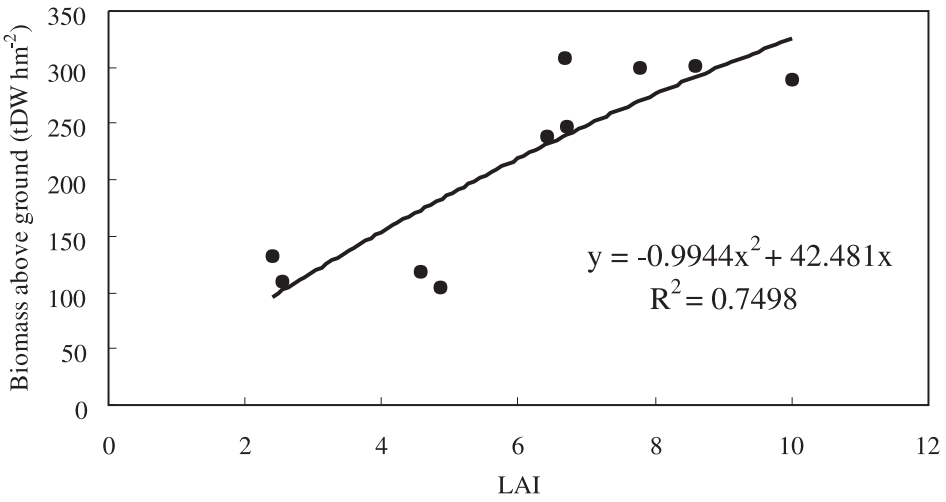

Figure 6. Relationship between LAI and aboveground biomass for forest vegetation.

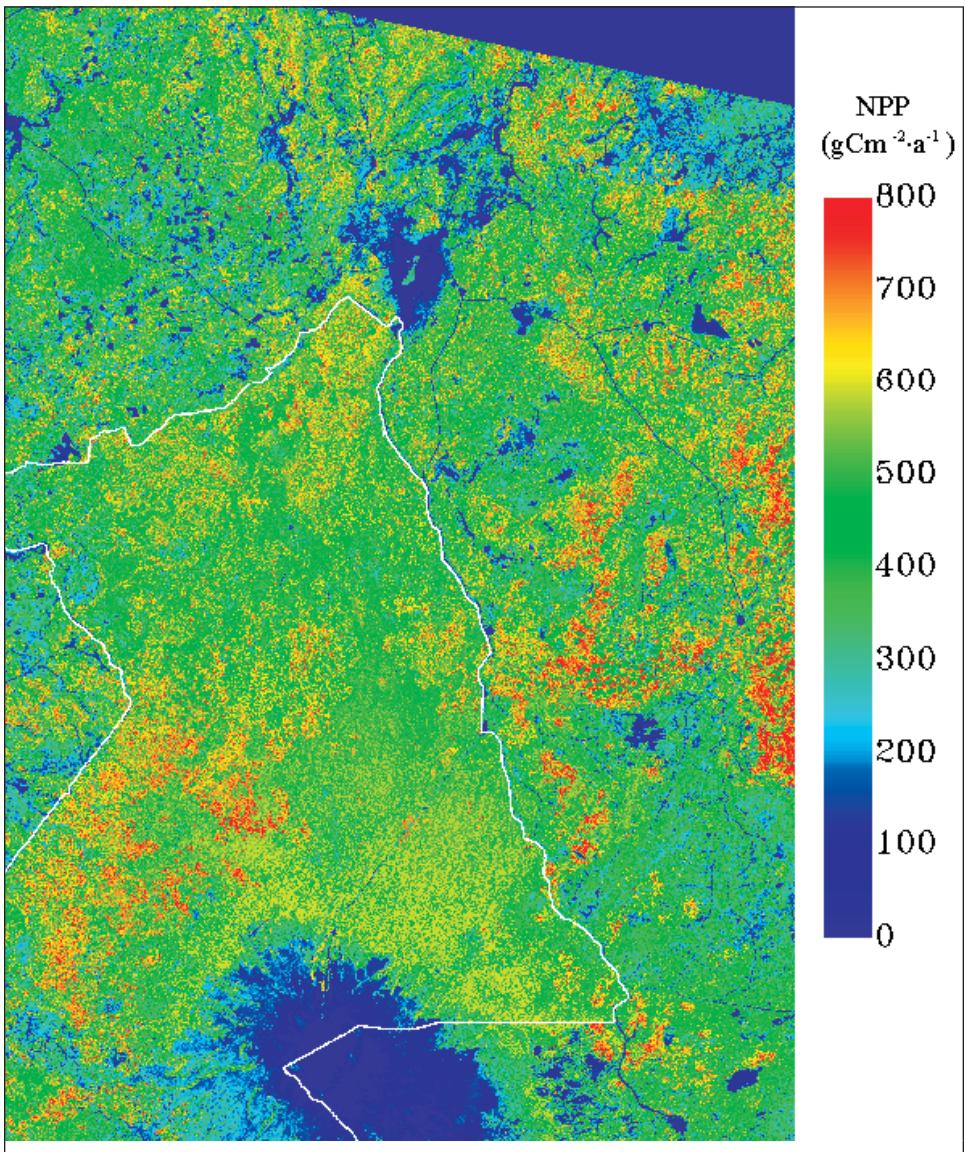

Figure 7. Spatial pattern of annual net primary productivity (NPP) on the north slope of Changbaishan Natural Reserve in 2001.

Annual NPP

Figure 7 shows the spatial pattern of annual NPP in the north slope of Changbaishan Natural Reserve in 2001. The annual NPP of forest mainly ranges from 400 to 600 g C $m^{-2}{\cdot}a^{-1}$, with the highest values greater than 800 g C $m^{-2}{\cdot}a^{-1}$. The highest NPP located in the west part of the study area, where the forest is Korean pine and broadleaf mixed forest, NPP is higher than 700 g C $m^{-2}{\cdot}a^{-1}$. The NPP of coniferous forest within the Changbaishan Natural Reserve is also high, with values ranging from 500 to 700 g C $m^{-2}{\cdot}a^{-1}$, whereas outside the reserve (e.g., in the lower right corner of the image in **Figure 7**) the NPP is low (less than 400 g C $m^{-2}{\cdot}a^{-1}$, which may be caused by human activities). Affected by the cold climate, NPP around Tianchi Lake is very low, and it is mostly less than 100 g C $m^{-2}{\cdot}a^{-1}$.

Among all vegetation types, mixed forest has the highest NPP, with a mean annual NPP of up to 500 g C $m^{-2}{\cdot}a^{-1}$; coniferous forest has the next highest NPP, and broadleaf forest has the lowest NPP (440 g C $m^{-2}{\cdot}a^{-1}$) among the forest types (**Table 1**). NPP of alpine tundra and shrub is the lowest in the

Table 1. Annual NPP for different vegetation types on the north slope of Changbaishan Natural Reserve in 2001.

Vegetation type	Mean NPP (g C $m^{-2}{\cdot}a^{-1}$)	Standard error of NPP (g C $m^{-2}{\cdot}a^{-1}$)	Ra/GPP (%)
Broadleaf forest	440	141	53.4
Coniferous forest	451	92	46.7
Mixed forest	500	141	48.9
Crop	232	108	55.8
Alpine tundra and shrub	136	111	31.8

Note: Ra is autotrophic respiration, including the maintenance respiration and growth respiration. GPP is gross primary productivity.

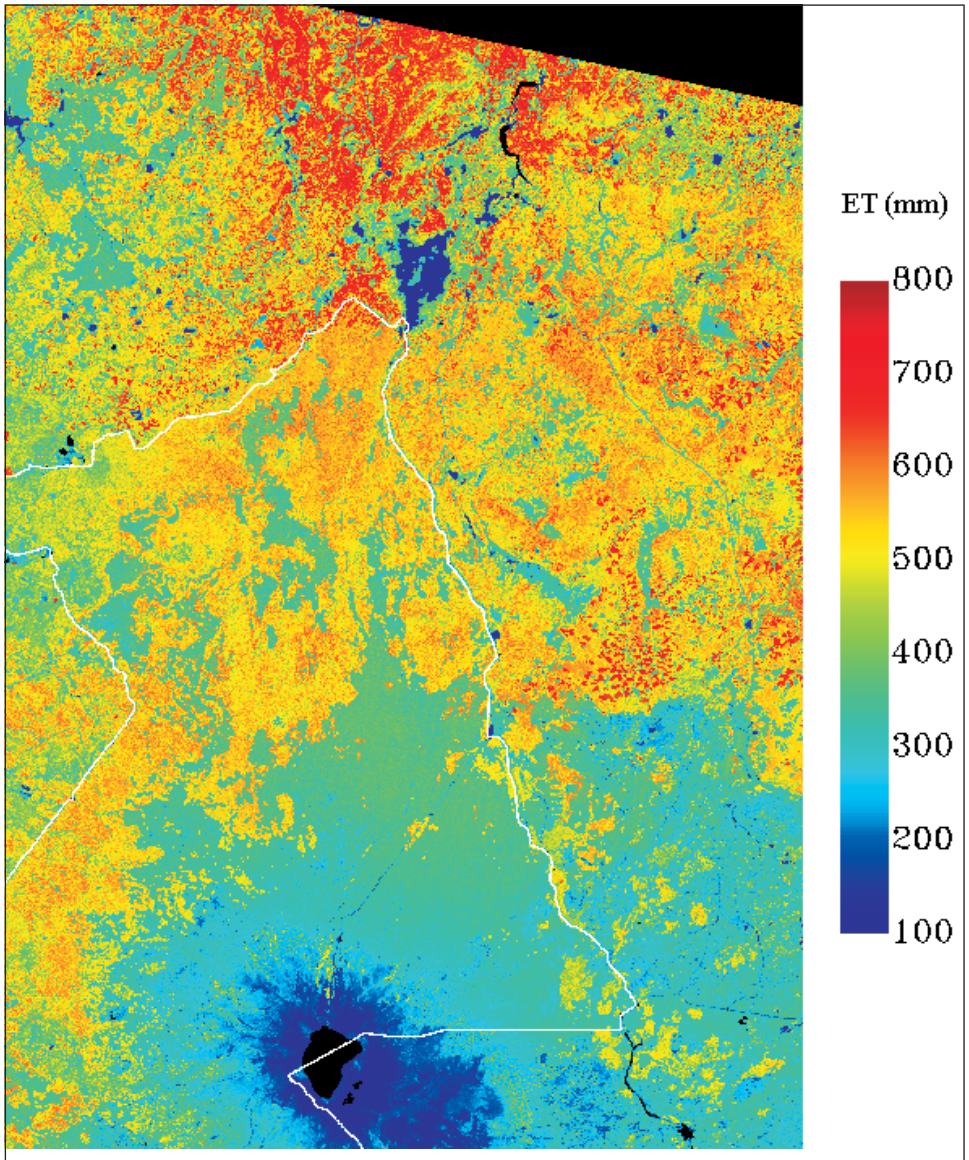

Figure 8. Spatial pattern of annual evapotranspiration (ET) on the north slope of Changbaishan Natural Reserve in 2001.

area, having a mean value of 136 g C $m^{-2}\cdot a^{-1}$. The NPP of crops is 232 g C $m^{-2}\cdot a^{-1}$, which is a little lower than the results of Chen et al. (2002a). There may be two reasons for the low NPP values for crops. First, the climate here is cold and the growing season is short. Second, a large part of the cropland is used for planting ginseng. The plastic sheds covering the ginseng increase the reflectance and add a negative bias to the LAI derived from remote sensing data, resulting in the low estimation of NPP. In addition, we used Equation (4) to estimate LAI of crops, even though the equation was developed based on Canadian crop data. Different soil backgrounds may induce biases in the LAI estimation.

Annual ET

Figure 8 shows the spatial pattern of annual evapotranspiration (ET) in the study area. Because ET of a water body was not calculated in the BEPS model, we use black to represent water bodies. **Figure 8** shows that the annual ET changes distinctly with changes in altitude. It is different from the rainfall distribution. ET changes from greater than 600 mm at the foot of the mountain to about 200 mm at the top of the mountain, whereas the rainfall changes from less than 700 mm at the foot of the mountain to more than 1100 mm at the top of the mountain. For different vegetation types, ET of broadleaf forest is the highest, with a mean of 566 mm·a^{-1} (**Table 2**). The mean annual ET of mixed forest decreases to 510 mm, whereas the ET for coniferous forest is just 333 mm. ET for crops is relatively high, with a mean annual value of 469 mm. However, the ET of crops is lower than that of forests in the same zone. The ET of urban and built-up areas is the lowest, with a mean annual value of just 110 mm.

The spatial distribution of ET does not show the same pattern as NPP across this large elevation range, especially in the forest region. Several processes can cause the difference in the spatial patterns of NPP and ET:

(1) Autotrophic respiration, which is highly dependent on temperature and biomass — Because the annual temperature distribution is significantly affected by the elevation, the ratio of autotrophic respiration (Ra) to gross primary productivity (GPP) also varies greatly with elevation. This ratio is shown in **Table 1**. **Table 1** shows that the ratio of Ra to GPP decreases with an increase in elevation. The ratio is highest for crop and broadleaf forest, which are mainly located at low elevations. The ratio for coniferous forest, which is mainly located at high elevations, is the lowest of the forest vegetation types. Both Ra/GPP and GPP for coniferous forest are lower than those for broadleaf forest, which results in the difference of spatial pattern between NPP and GPP. As the water and carbon flows through stomata in leaves are controlled by consistent stomatal conductances (1.6 times smaller for the carbon flow) in the BEPS model, the transpiration and GPP are tightly coupled. Therefore, the transpiration obviously decreases with an increase in elevation.

(2) Interceptional water loss and evaporation from soil surface — The interceptional water loss depends on precipitation and LAI. Because the precipitation and LAI increase with an increase in elevation in the forest region, evaporation from the canopy also increases with an increase in elevation. Evaporation from a soil surface varies little with elevation because the forest region is fully covered by the canopy. The evaporation modeled from BEPS increases slightly with an increase in elevation in the forest region. Because the change range of evaporation is small, the spatial pattern of ET mainly depends on transpiration.

Validation of NPP

Comparing the modeled NPP with ground-based data (**Figure 9**; **Table 3**), we found that, although the modeled NPP of forest is higher than the observed NPP, with a mean relative error of 8.6% and the largest error of 36.8%, they are consistent with each other. The correlation coefficient is up to 0.90. The results demonstrate that the NPP map (**Figure 7**) has a

Table 2. Annual ET for different land cover types on the north slope of Changbaishan Natural Reserve in 2001.

Vegetation type	Mean ET (mm)	Standard error (mm)
Broadleaf forest	566	124
Coniferous forest	333	35
Mixed forest	510	70
Crop	469	128
Alpine tundra and shrub	216	82
Urban and built-up	110	5

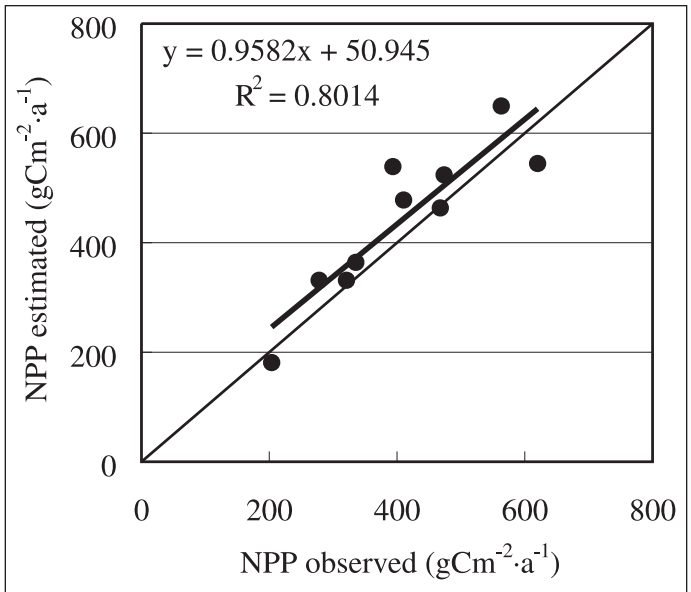

Figure 9. Comparison between observed NPP and NPP estimated using the BEPS model.

Table 3. Comparison between the modeled and field-observed NPP in 2001.

Site	Forest type	Field NPP (g C $m^{-1}{\cdot}a^{-1}$)	Modeled NPP (g C $m^{-1}{\cdot}a^{-1}$)	Relative error (%)
1	Korean pine and deciduous broadleaf forest	563.2	650.0	15.4
2	*Pinus sylvestriformis* forest	278.2	331.5	19.1
3	Poplar and birch forest	321.0	331.6	3.3
4	Poplar and birch forest	335.7	364.3	8.5
5	*Betula ermanii* forest	203.6	181.0	–11.1
6	Spruce and fir forest	473.5	523.8	10.6
7	*Betula ermanii* and spruce and fir forest	393.7	538.7	36.8
8	Korean pine and spruce and fir forest	619.9	544.5	–12.2
9	Korean pine and deciduous broadleaf forest	467.9	463.8	–0.9
10	Deciduous pine and fir forest	410.4	477.8	16.4
Mean		406.7	440.7	8.6

reasonable accuracy of at least better than 75% for remote sensing applications (Liu et al., 2002).

Conclusion

Based on field data and Landsat ETM+ images, the BEPS model was successfully used to produce net primary productivity (NPP) and evapotranspiration (ET) maps in Changbaishan Natural Reserve, China. The results show that the modeled and observed NPP of forests agree fairly well, with a mean relative error of 8.6%, demonstrating that BEPS can be effectively used to estimate NPP of forests using high-resolution images. As BEPS has only been applied to coarse-resolution images, our study further confirms that remote sensing images are indeed useful for the study of terrestrial water and carbon cycles.

The NPP of forests in the study area mainly ranges from 400 to 600 g C $m^{-2}{\cdot}a^{-1}$. The NPP of mixed forest is the highest, with a mean of 500 g C $m^{-2}{\cdot}a^{-1}$, and that of alpine tundra and shrub is the lowest, with a mean of 136 g C $m^{-2}{\cdot}a^{-1}$.

Unlike the spatial pattern of NPP, the annual ET changes distinctly with a change in elevation. ET decreases from greater than 600 mm at the foot of the mountain to about 200 mm at the top. ET is highest for broadleaf forest and lowest for urban and built-up areas.

Acknowledgments

The study was funded by the Canadian International Development Agency (CIDA) and the Chinese National Key Research Program of Basic Science (grants G2000077908 and G2000077906 and Ministry of Science and Technology of China grant 2001CB309404). The authors thank Dr. Mingzhen Chen and Mr. Feng Deng of the University of Toronto for help with the atmospheric correction. Professor Xuezheng Shi of the Institute of Soil Science, Chinese Academy of Sciences, is greatly acknowledged for supplying the soil texture map. The authors also thank those who participated in the field experiment, including Menxin Wu, Jun Qin, Xin Wei, Xianfeng Feng, Li Li, and Shiqi Yang.

References

Asrar, G., Fuchs, M., Kanemasu, E.T., and Hatfield, J.L. 1984. Estimating absorbed photosynthetically active radiation and leaf area index from spectral reflectance in wheat. *Agronomy Journal*, Vol. 76, pp. 300–306.

Bartlett, D.S., Whiting, G.J., and Hartmann, J.M. 1990. Use of vegetation indices to estimate intercepted solar radiation and net carbon dioxide exchange of a grass canopy. *Remote Sensing of Environment*, Vol. 30, pp. 115–128.

Bonan, G.B. 1995. Land–atmosphere CO_2 exchange simulated by a land surface process model coupled to an atmospheric general circulation model. *Journal of Geophysical Research*, Vol. 100, No. D2, pp. 2817–2831.

Box, E.O. 1988. Estimating the seasonal carbon source–sink geography of a natural, steady-state terrestrial biosphere. *Journal of Applied Meteorology*, Vol. 27, pp. 1109–1124.

Brown, L.J., Chen, J.M., Leblanc, S.G., and Cihlar, J. 2000. Short wave infrared correction to the simple ratio: an image and model analysis. *Remote Sensing of Environment*, Vol. 71, pp. 16–25.

Chen, C.G., and Zhu, J.F. 1989. *The manual of forest biomass in northeast of China*. Chinese Forestry Press, Beijing, China.

Chen, J.M., Liu, J., Cihlar, J., and Goulden, M.L. 1999. Daily canopy photosynthesis model through temporal and spatial scaling for remote sensing applications. *Ecological Modelling*, Vol. 124, pp. 99–119.

Chen, L.J., Liu, G.H., and Li, H.G. 2002a. Estimating net primary productivity of terrestrial vegetation in China using remote sensing. *Journal of Remote Sensing*, Vol. 6, No. 2, pp. 129–135.

Chen, J.M., Pavlic, G., Brown, L., Cihlar, J., Leblanc, S.G., White, H.P., Hall, R.J., Peddle, D.R., King, D.J., Trofymow, J.A., Swift, E., Van der Sanden, J., and Pellikka, P.K.E. 2002b. Derivation and validation of Canada-wide coarse-resolution leaf area index maps using high-resolution satellite imagery and ground measurements. *Remote Sensing of Environment*, Vol. 80, pp. 165–184.

Chen, J.M., Liu, J., Leblanc, S.G., Lacaze, R., and Roujean, J.L. 2003. Multi-angular optical remote sensing for assessing vegetation structure and carbon absorption. *Remote Sensing of Environment*, Vol. 84, pp. 516–525.

Farquhar, G.D., von Caemmerer, S., and Berry, J.A. 1980. A biochemical model of photosynthetic CO_2 assimilation in leaves of C_3 species. *Planta*, Vol. 149, pp. 78–90.

Feng, Z.W., Wang, X.K., and Wu, G. 1999. *Biomass and productivity of forest ecosystem in China*. Sciences Press, Beijing, China.

Field, C.B., Randerson, J.T., and Malmstrom, C.M. 1995. Global net primary production: combining ecology and remote sensing. *Remote Sensing of Environment*, Vol. 51, pp. 74–88.

Foley, J.A. 1994. Net primary productivity in the terrestrial biosphere: the application of a global model. *Journal of Geophysical Research*, Vol. 99, No. D10, pp. 20 773 – 20 783.

Fung, I.Y., Tucker, C.J., and Prentice, K.C. 1987. Application of advanced very high resolution radiometer vegetation index to study atmosphere–biosphere exchange of CO_2. *Journal of Geophysical Research*, Vol. 92, pp. 2999–3015.

Gallo, K.P., Daughtry, C.S.T., and Bauer, M.E. 1985. Spectral estimation on absorbed photosynthetically active radiation in corn canopies. *Remote Sensing of Environment*, Vol. 17, pp. 221–232.

King, A.W., O'Neill, R.V., and DeAngelis, D.L. 1989. Using ecosystem models to predict regional CO_2 exchange between the atmosphere and the terrestrial biosphere. *Global Biogeochemical Cycles*, Vol. 3, pp. 337–361.

Law, B.E., and Waring, R.H. 1994. Combining remote sensing and climatic data to estimate net primary production across Oregon. *Ecological Applications*, Vol. 4, pp. 717–728.

Li, D.Q., Sun, C.Y., and Zhang, X.S. 1998. Modelling the net primary productivity of the natural potential vegetation in China. *Acta Botanica Sinica*, Vol. 40, No. 6, pp. 560–566.

Lieth, H., and Whittaker, R.H. 1975. *Primary productivity of the biosphere.* Springer-Verlag, New York.

Liu, J., Chen, J.M., Cihlar, J., and Park, W.M. 1997. A process-based boreal ecosystem productivity simulator using remote sensing inputs. *Remote Sensing of Environment*, Vol. 62, pp. 158–175.

Liu, J., Chen, J.M., Cihlar, J., and Chen, W. 2002. Net primary productivity mapped for Canada at 1-km resolution. *Global Ecology and Biogeography*, Vol. 11, pp. 115–129.

Lu, J.H., and Ji, J.J. 2002. A simulation study of atmosphere–vegetation interaction over the Tibetan Plateau, part II: net primary productivity and leaf area index. *Chinese Journal of Atmospheric Sciences*, Vol. 26, No. 2, pp. 255–262.

Luo, T.X., Li, W.H., Leng, Y.F., and Yue, Y.Z. 1998. Estimation of total biomass and potential distribution of net primary productivity in the Tibetan Plateau. *Geographical Research*, Vol. 17, No. 6, pp. 337–344.

Melillo, J.M., McGuire, A.D., Kicklighter, D.W., Moore, B., III, Vörösmarty, C.J., and Schloss, A.L. 1993. Global climate change and terrestrial net primary production. *Nature (London)*, Vol. 363, pp. 234–240.

Piao, S.L., Fang, J.Y., and Guo, Q.H. 2001. Application of CASA model to the estimation of Chinese terrestrial net primary productivity. *Acta Phytoecologica Sinica*, Vol. 25, No. 5, pp. 603–608.

Potter, C.S., Randerson, J.T., Field, C.B., Matson, P.A., Vitousek, P.M., Mooney, H.A., and Klooster, S.A. 1993. Terrestrial ecosystem production: a process model based on global satellite and surface data. *Global Biogeochemical Cycles*, Vol. 7, pp. 811–841.

Prince, S.D., and Goward, S.N. 1995. Global primary production: a remote sensing approach. *Journal of Biogeography*, Vol. 22, pp. 815–835.

Raich, J.W., Pastetter, E.B., Melillo, J.M., Kicklighter, D.W., Grace, P.A., Moore, B., and Peterson, B.J. 1991. Potential net primary productivity in South America: application of a global model. *Ecological Applications*, Vol. 1, pp. 399–429.

Rosenzweig, M.L. 1968. Net primary productivity of terrestrial communities: prediction from climatological data. *American Naturalist*, Vol. 102, pp. 67–74.

Ruimy, A., and Saugier, B. 1994. Methodology for the estimation of terrestrial net primary production from remotely sensed data. *Journal of Geophysical Research*, Vol. 99, No. D3, pp. 5263–5283.

Running, S.W., and Coughlan, J.C. 1988. A general model of forest ecosystem processes for regional applications: I. Hydrological balance, canopy gas exchange and primary production processes. *Ecological Modelling*, Vol. 42, pp. 125–154.

Ryan, M.G. 1991. A simple method for estimating gross carbon budgets for vegetation in forest ecosystems. *Tree Physiology*, Vol. 9, pp. 255–266.

Saxton, K.E., Rawals, J.W., Romberger, J.S., and Papendick, R.I. 1986. Estimating generalized soil-water characteristics from texture. *Soil Science Society of America Journal*, Vol. 50, pp. 1031–1036.

Sellers, P.J., Los, S.O., Tucker, C.J., Justice, C.O., Dazlich, D.A., Collatz, G.J., and Randall, D.A. 1996. A revised land surface parameterization (SiB2) for atmospheric GCMs. Part II: the generation of global fields of terrestrial biophysical parameters from satellite data. *Journal of Climate*, Vol. 9, pp. 706–737.

Sun, R., and Zhu, Q.J. 2001. Estimation of net primary productivity in China using remote sensing data. *Journal of Geographical Sciences*, Vol. 11, No. 1, pp. 14–23.

Uchijima, Z., and Seino, H. 1985. Agroclimatic evaluation of net primary productivity of nature vegetation (1). Chikugo model for evaluating primary productivity. *Journal of Agricultural Meteorology*, Vol. 40, pp. 343–352.

Vermote, E., Tanre, D., Deuze, J.L., Herman, M., and Morcrette, J.J. 1997. *Second simulation of the satellite signal in the solar spectrum (6S), 6S user guide version 1*. NASA Goddard Space Flight Center, Greenbelt, Md.

Weng, D.M., and Sun, Z.A. 1984. A preliminary study of the lapse rate of surface air temperature over mountainous regions of China. *Geographical Research*, Vol. 3, No. 2, pp. 24–34.

Winslow, J.C., Hunt, E.R., Jr., and Piper, S.C. 2001. A globally applicable model of daily solar irradiance estimated from air temperature and precipitation data. *Ecological Modelling*, Vol. 143, pp. 227–243.

Yu, M., Gao, Q., Xu, H.M., and Liu, Y.H. 2001. Response of vegetation distribution and primary production of the terrestrial ecosystems of China to climatic change. *Quaternary Science*, Vol. 21, No. 4, pp. 281–293.

Zhang, N., Yu, G.R., Zhao, S.D., and Yu, Z.L. 2003. Ecosystem productivity process model for landscape based on remote sensing and surface data. *Chinese Journal of Applied Ecology*, Vol. 14, No. 5, pp. 643–652.

Zhou, G.S., and Zhang, X.S. 1996. Study on NPP of natural vegetation in China under global climate change. *Acta Phytoecologica Sinica*, Vol. 20, No. 1, pp. 11–19.

Zhu, Z.H. 1993. A model for estimating net primary productivity of natural vegetation. *Chinese Science Bulletin*, Vol. 38, No. 15, pp. 1422–1426.